

Expediting quantum state transfer through long-range extended XY model

Sejal Ahuja¹, Tanoy Kanti Konar¹, Leela Ganesh Chandra Lakkaraju^{1,2}, Aditi Sen(De)¹

¹*Harish-Chandra Research Institute, A CI of Homi Bhabha National Institute,
Chhatnag Road, Jhansi, Allahabad - 211019, India and*

²*Pitaevskii BEC Center and Department of Physics, University of Trento, Via Sommarive 14, I-38123 Trento, Italy*

Going beyond short-range interactions, we explore the role of long-range interactions in the extended XY model for transferring quantum states through evolution. In particular, employing a spin-1/2 chain with interactions decaying as a power law, we demonstrate that long-range interactions significantly enhance the efficiency of a quantum state transfer (QST) protocol, reducing the minimum time required to achieve fidelity beyond the classical limit. Our study identifies the long-range regime as providing an optimal balance between interaction range and transfer efficiency, outperforming the protocol with the short-range interacting model. Our detailed analysis reveals the impact of system parameters, such as anisotropy, magnetic field strength, and coordination number, on QST dynamics. Specifically, we find that intermediate coordination numbers lead to a faster and more reliable state transfer, while extreme values diminish performance. Further, we exhibit that the presence of long-range interactions also improves the achievable fidelity, mitigating its decline associated with increasing system-size.

I. INTRODUCTION

Quantum technology presents an exciting avenue for the development of advanced devices, such as communication systems [1–3] including cryptography [4, 5], quantum batteries [6, 7], sensors [8, 9], that could significantly surpass the performance of existing classical counterparts. One essential component in quantum networks and circuits is the transmission of information through quantum channels, known as quantum state transfer (QST). In this framework, physical systems such as engineered spin chains in condensed matter systems have emerged as effective data buses [10–12], facilitating the transmission of quantum information between different nodes which has been shown in different setup [13–26]. When these spin chains are carefully engineered, they can achieve perfect quantum state transfer under specific conditions [27–35]. The key to this process lies in the presence of a notable spin gap, which greatly enhances the system’s ability to reliably transmit quantum states. This gap ensures that the interaction between two spins at the ends of the chain can be described by an effective Hamiltonian, resembling that of a Heisenberg-type interaction [36]. This promising approach demonstrates the potential of spin chains as well as several different physical substrates, e.g. photonic systems [37, 38], superconducting circuits [39] for quantum state transfer, offering valuable insights for future advancements in quantum communication technology.

Long-range interacting Hamiltonian exhibit counter-intuitive phenomena, including many-body localization [40], alterations in the Lieb-Robinson bound due to the induction of long-range (LR) correlations [41], and exotic quantum phases and transitions [42]. These features make long-range systems highly promising for the development of quantum technologies like heat engines, batteries, sensors, and more [43–46]. Moreover, in trapped ion systems, ions can interact with each other via collective modes of motion, which naturally results in long-range interactions [47, 48] while dipolar interactions or the use of optical fields that mediate spin interactions over long distances can be used to engineer cold atoms in optical lattices to display LR interactions [49]. Hence, these LR systems are not only theoretically intriguing

but also experimentally accessible on current platforms.

Even though the potential of long-range (LR) interacting systems has been widely recognized through the development of various quantum devices, their application in quantum state transfer remains largely underexplored [50–54]. Notably, specific LR interactions have been shown to enable perfect QST [30, 33]; nevertheless realizing such Hamiltonian in practical experimental setups is quite challenging. Therefore, it is essential to study LR interacting systems in realistic scenarios and demonstrate their ability to perform efficient QST [55]. Moreover, it is crucial to explore whether they can outperform systems relying solely on nearest-neighbor (NN) interactions.

To address these challenges, we focus on the extended XY model [56, 57], involving N -body interactions that decay with distance, exhibiting two transitions, from long- to quasi long-range and quasi long- to short-range regimes. Further, it can be solved analytically using Jordan-Wigner, Fourier, and Bogoliubov transformations [58–61], enabling its investigation for large system sizes. Importantly, it has been shown to be experimentally realizable on platforms such as optical lattices and trapped ion systems [42]. Recently, experiments with more than two-body interactions have been studied in the context of quantum approximate and optimization algorithms [62]. Specifically, three-body ZZZ -interaction has been realized in superconducting [63, 64] and quantum annealing platforms [65]. By leveraging this model, we establish the potential of LR interactions for robust and efficient quantum state transfer. We employ two key figures of merits: the minimum time required to achieve fidelity beyond the classical limit and the maximum fidelity achieved for the first time.

We exhibit that there is always a coordination number incorporating long-distant interactions that requires less time to surpass the classical fidelity, in comparison to systems with solely NN interactions. However, our investigations indicate that this quantum advantage is highly dependent on the system parameters, necessitating careful selection of these parameters for optimal performance. We identify that the quasi long-range interaction regime offers a distinct advantage over the deep long- and short-range interacting systems. This suggests that there exists an optimal range of

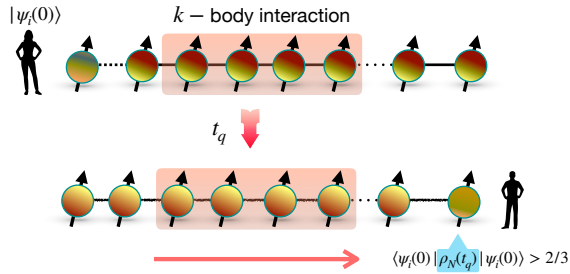


FIG. 1. Schematic diagram illustrating quantum state transfer. The first spin in the first line possessed by Alice is the arbitrary state to be transferred while the rest of the sites representing the spin chain involving k -body interactions acted as a quantum channel. After a time t_q (second line), the state transfer occurs since the fidelity of the last site crosses the classical limit, $2/3$.

long-range interaction strength that is particularly beneficial for QST protocols. Moreover, we analyze the impact of system-size on the average fidelity of QST. While fidelity decreases with increasing system-size, our findings reveal that in systems with long-range interactions, this reduction is slower. The rate of decline in fidelity depends on the strength of the long-range interactions, further emphasizing the role of long-range effects in mitigating the challenges posed by larger system sizes. Overall, our study highlights the critical role of long-range interactions, coordination number, and system parameters in enhancing QST performance. By carefully tuning these factors, it is possible to exploit the exotic properties of the extended XY model to achieve efficient quantum state transfer, even in larger systems. This work provides valuable insights into the practical utility of long-range interactions and offers guidance for designing QST protocols leveraging extended XY models.

The paper is organized in the following manner. Sec. II introduces the set-up to achieve the successful state transmission protocol with the aid of evolving interacting Hamiltonian. The results are presented in Secs. III and IV. In the former section, we demonstrate how the minimum time to achieve nonclassical fidelity depends on the range of interaction and fall-off rates. Sec. IV addresses the question of maximum fidelity that can be attained with the LR spin model used during the dynamics and its scaling with the length of the spin chain. Sec. V summarizes the results and concluding remarks.

II. A LONG-RANGE SPIN MODEL AS A QUANTUM CHANNEL FOR STATE-TRANSMISSION

In a seminal work of quantum teleportation [1], it was shown that a sender, say Alice, A can send an arbitrary quantum state (say, qubit) to the receiver, say Bob, B provided they a priori share an entangled quantum channel. Note that if Alice and Bob do not share any entangled quantum channel, the transmission of an arbitrary qubit cannot be possible over the fidelity $2/3$ which we refer to the classical fidelity

[66]. Importantly, this protocol requires entangled measurement at the sender's end while local unitaries at the receiver's side have to be performed after classical communication of Alice's measurement results.

On the other hand, in the state transfer protocol [10], the measurement and local unitary is replaced by the evolution of the system by a suitable Hamiltonian, although the goal is same in both the protocols. The dynamical state entangles all the spins, thereby acting as an entangled quantum channel, responsible for the transfer of quantum state from one site to the other.

Let us set the stage for the protocol. First, prepare an arbitrary state $|\psi(0)\rangle$, which is to be transferred, at the first site of the chain consisting of N spin- $1/2$ particles which interact according to some Hamiltonian $\hat{\mathcal{H}}$. Initially, the $(N-1)$ -party state is prepared in the ground or canonical equilibrium state of $\hat{\mathcal{H}}$, i.e., at time $t = 0$,

$$\hat{\rho}(0) = |\psi(0)\rangle\langle\psi(0)| \otimes \rho^\beta(0) \quad (1)$$

where $\rho^\beta(0) = e^{-\beta\hat{\mathcal{H}}}/\mathcal{Z}$ with the partition function $\mathcal{Z} = \text{tr}(e^{-\beta\hat{\mathcal{H}}})$, and $\beta = 1/k_B T$ having temperature T and Boltzmann constant k_B , represents the $(N-1)$ -party thermal state of $\hat{\mathcal{H}}$ acting as a quantum channel for state transmission. In our analysis, we consider the thermal state with $\beta \rightarrow \infty$, i.e., when the system is in a ground state of $\hat{\mathcal{H}}$. Let us now evolve N sites according to $\hat{\mathcal{H}}$, resulting in a N -party state as $|\psi_N(t)\rangle = e^{-i\hat{\mathcal{H}}t}[|\psi(0)\rangle \otimes |\Psi(0)\rangle]$, where $|\Psi(0)\rangle$ is the $(N-1)$ -party ground state of the Hamiltonian. At a suitable time, by tracing out $(N-1)$ parties from $|\psi_N(t)\rangle$, the resulting state, $\rho_N(t)$, at the site N is compared with the initial state $|\psi(0)\rangle$ at the first site by computing the average fidelity,

$$f = \int \langle \psi(0) | \rho_N(t) | \psi(0) \rangle d|\psi(0)\rangle \\ = \frac{1}{4\pi} \int_{\theta=0}^{\pi} \int_{\phi=0}^{2\pi} \langle \psi(0) | \rho_N(t) | \psi(0) \rangle \sin \theta d\theta d\phi, \quad (2)$$

where in the first line, the integral is taken over the entire Bloch sphere and the second line is written by parametrizing the initial state as $|\psi(0)\rangle = \cos \theta/2|0\rangle + e^{i\phi} \sin \theta/2|1\rangle$. A state transfer protocol is called successful when $f > 2/3$, as it is known that without an entangled channel, state cannot be transferred with a fidelity greater than $2/3$ [67], referred to as the classical fidelity or limit. This criterion distinguishes quantum protocols from their classical counterparts, establishing $f > 2/3$ as a necessary condition for demonstrating *quantum advantage*.

It is clear that the entire protocol depends on the initial preparation of the $(N-1)$ -party state, the evolution operator, thereby depending on the Hamiltonian, time and the length of the chain N . Typically, the Hamiltonian responsible for the unitary dynamics involves nearest-neighbor interactions [10, 68]. In our work, the Hamiltonian involving long-range

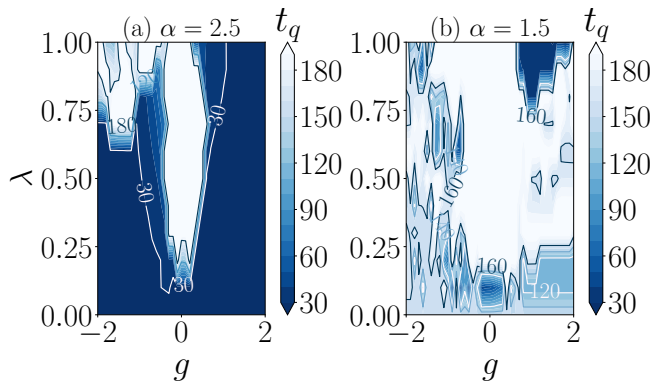


FIG. 2. Contour plot of minimum time required to achieve classical fidelity, t_q against system parameters, g and λ . (a) $\alpha = 2.5$ and (b) $\alpha = 1.5$. Here $z = N - 1$ and $N = 25$. It is evident that the choice of (λ, g) for the short-range models is different than the long-range ones. All the axes are dimensionless.

interacting XY -model is considered, given by [57]

$$\hat{\mathcal{H}} = \sum_{j=1}^N \sum_{\delta=1}^z -\mathcal{J}_{\delta} \left[\frac{1+\lambda}{4} \hat{S}_j^x \hat{Z}_{\delta}^z \hat{S}_{j+\delta}^x + \frac{1-\lambda}{4} \hat{S}_j^y \hat{Z}_{\delta}^z \hat{S}_{j+\delta}^y \right] - \frac{g'}{2} \sum_{j=1}^N \hat{S}_j^z. \quad (3)$$

Here, $\hat{Z}_{\delta}^z = \prod_{l=j+1}^{j+\delta-1} \hat{S}_l^z$ represents the string operator with $\hat{Z}_1^z = \hat{\mathbb{1}}$, and \hat{S}^k ($k = x, y, z$) are the Pauli matrices. The coupling strength follows a power-law decay, $\mathcal{J}_{\delta} = \frac{J}{\delta^{\alpha}}$, where α characterizes the decay strength. The coordination number z determines the range of interactions, analogous to the crystal structures in solid-state systems. When $\alpha \rightarrow \infty$, the system reduces to nearest-neighbor interactions, while $\alpha = 0$ corresponds to z -neighbor interactions. The parameter λ controls the anisotropy in the xy -plane, and g represents the strength of the transverse magnetic field. Note that the Kac normalization is not applicable in our context, as we focus mostly on the regime of $\alpha > 1$, where the physics described by both ‘‘Kac on’’ and ‘‘Kac off’’ models is similar [42]. The advantage of using the Kac normalization is to obtain non-divergent observables in the thermodynamic limit. However, in the context of quantum state transfer, the $N \rightarrow \infty$ limit is inconsequential, as it cannot provide a quantum advantage. To make the parameters dimensionless, the strength of the magnetic field is rescaled as $g = g'/J$. It is interesting to note that such a system undergoes transition with respect to α which is different than quantum phase transition [61]. Specifically, correlation length [56, 57], entanglement [69] and information spreading via Lieb-Robinson bounds [70] can detect these transition points, and reveal that the system possesses long-range when $0 \leq \alpha \leq 1$, quasi long-range with $1 < \alpha \leq 2$ and short-range for $\alpha > 2$.

III. LESS TIME TO ACHIEVE QUANTUM ADVANTAGE THROUGH LONG-RANGE INTERACTIONS

Consider a situation where the goal is to transfer an arbitrary quantum state over a chain of fixed length, say, N via dynamics. Due to a finite size, information transmission can occur several times which implies that the fidelity oscillates over the time of evolution. From a practical perspective, it is intriguing to determine the minimum time in which the average fidelity goes beyond $2/3$ for a fixed length of a spin chain, thus ensuring a *quantum advantage*. We denote this time by t_q . To find t_q , we compute the lowest time when $f - \frac{2}{3} > \epsilon$, where ϵ is a small positive number. In our analysis, $\epsilon \sim 10^{-4}$. This figure of merit can be attributed to the basic necessity for transferring quantum states. We will analyze how t_q depends on the system parameters, especially when the variable-range interacting XY spin model, in Eq. (3), is used to evolve the system (see Appendix A for diagonalization method of the model and B for the computation of fidelity). In particular, we connect t_q with the coordination number z and the fall-off rate of the interaction strength, α along with the magnetic field strength g , and anisotropy λ for a fixed system-size, N . Since we are interested in studying the state transfer protocol, it also depends crucially on the length of the chain N which we will also address. The entire analysis can reveal whether the LR interacting model has any beneficial role for transferring quantum states through evolution.

A. Crucial role of system parameters in quantum advantage

In order to determine how system parameters of $\hat{\mathcal{H}} \equiv \hat{\mathcal{H}}(N, z, \alpha, \lambda, g)$ can change the minimum time to obtain quantum advantage, we deal with a chain of fixed length N , which is typical in current experimental realizations of quantum circuits. The analysis focuses on chains with lengths around $N \sim 20$ or $N \sim 30$. To make the study systematic, we further set three values of α , belonging to long-, quasi long- and short-range interacting model and two extreme z values *viz.*, $z = N - 1$, which corresponds to the interactions between any two arbitrary sites of the chain and $2 \leq z \leq N/2$, among which $z = 2$ involves nearest and next-nearest neighbor interactions. Note here that $z = 1$, representing Hamiltonian only with nearest neighbor interactions, does not have any α -dependence by definition. Hence, for a fixed N , α and z , the evolving Hamiltonian responsible for a state transfer is now a function of $\lambda \geq 0$ and $g \geq 0$ among which the XX model with $\lambda = 0$ does not depend on g [71].

Let us first notice that α does not play a significant role for obtaining minimum t_q when $z = 2$, i.e., the values in the λ, g -plane which are favorable for minimizing t_q with $\alpha > 2$ remains so even for low α values. For example, when $z = 2$ and $0 \leq \alpha \leq 2$, $t_q \leq 30$ for all values of λ and $|g|$ except few regions when the anisotropy is close to unity and $g < -1$. However, this is not the case for $|g| \ll 1$ with $\alpha \geq 2$, i.e., in this domain, even for $z = 2$, t_q turns out to be high except when the magnetic field strength is very small and $\lambda \simeq \lambda_c < 0.1$. Such observations can have an implication –

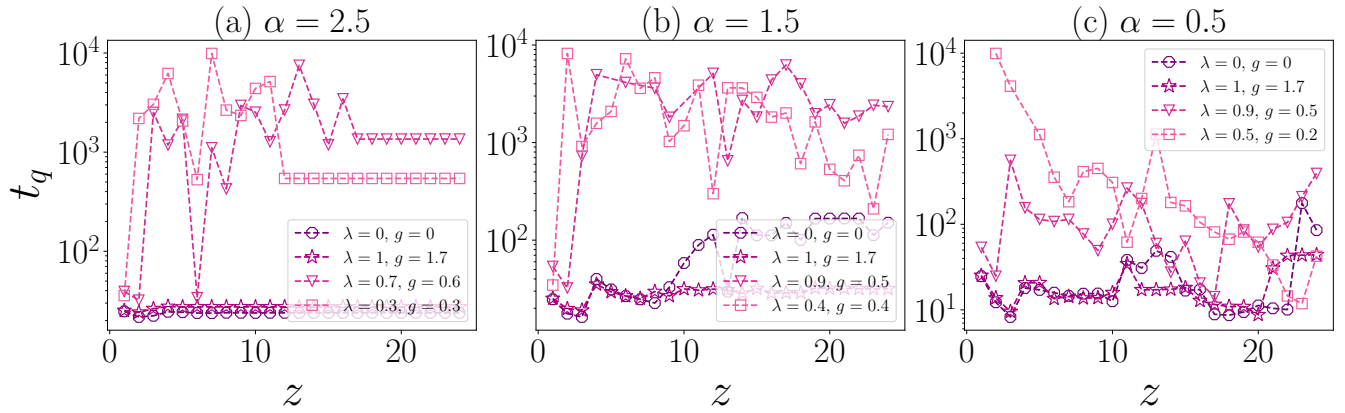


FIG. 3. Illustration of t_q (ordinate) versus coordination number z (abscissa) for the extended transverse XY model. To demonstrate, we choose four pairs of (λ, g) depicted in varying color shades, corresponding to three regimes of α (i.e., 2.5, 1.5, and 0.5), belonging to short-, quasi long- and long-range regimes. Here $N = 25$. The results highlight the preference for short- and long-range interactions across different regimes depending upon the choice of (λ, g) values. In both quasi long- and long-range domains, there always exists $z > 1$ values for which t_q is smaller than that obtained with $z = 1$, corresponding to NN interactions. All the axes are dimensionless.

the performance quantifiers for the state transfer protocol can distinguish $\alpha > 2$ and $\alpha \leq 2$ regimes. It is also important to note here that the analysis is performed with $N \leq 50$ and can be the artifact of finite-size systems which we will also address.

It is obvious that if one increases z values, t_q starts depending on α more crucially. For moderate z ($\sim N/2$), two observations emerge – (1) the region in the (λ, g) -plane which is good for obtaining low t_q with $z = 2$ remains the same when $\alpha \in [2, 3]$. (2) For $\alpha < 2$, $|g| > 1$ irrespective of the anisotropy parameters turn out to be appropriate for obtaining minimum time for quantum advantage.

In the case of $z = N - 1$, although the choices of λ and g values do not vary much with $z \sim N/2$, t_q here fluctuates with α and, in general, t_q increases. This can be due to the fact that the entanglement length of the ground state in the quasi long-range regimes is same as that obtained with short-range interactions although when $\alpha < 1$, entanglement length scales in a different manner [72].

B. Improvement of minimum time required to attain quantum advantage with coordination number

The above study helps us to identify an appropriate set of parameters, g and λ , to achieve a minimum t_q . Fixing the pair (λ, g) and N , we will now investigate the effect of LR interaction on state transfer by varying z and α . It is also evident from the above analysis that the quantum advantage can be obtained when both short- and long-range interacting Hamiltonian are used for dynamics. However, our goal is to find the ordering between $t_q^{0 < \alpha \leq 1}$, $t_q^{1 < \alpha \leq 2}$ and $t_q^{2 < \alpha \leq 3}$ where the superscripts denote the α values belonging to long-, quasi long- and short-range regimes. Since we are interested in a finite-size system and we also observe that $\alpha \geq 5$ actually mimics the results obtained with the nearest-neighbor Hamiltonian in the literature [71], we believe that when the fall-off rate belongs to the neighborhood of $\alpha = 2$, i.e., $\alpha \in [2 + \epsilon, 3 - \epsilon']$, where ϵ and ϵ' are small numbers, the

evolving Hamiltonian still carries some signature of the LR model. We will show that this is indeed true.

Short-range but close to quasi-LR domain. The minimum time to have quantum advantage has a universal feature with z for a fixed $2 \leq \alpha < 3$, and for all values of g and λ – initially, t_q decreases (increases) with z and then increases (decreases) before saturating to a fixed value, t_q^{sat} , for a high value of z . Since our aim is to highlight the benefit of LR interacting system, we always compare the result with $z = 1$. When $|g| < 1$, we observe that

$$t_q^{z=2} < t_q^{z=1}, \text{ and } t_q^{sat} < t_q^{z=1}, \quad (4)$$

independent of the anisotropy parameters, $\lambda \neq 0$. For example, $\lambda = 0.5$, $g = 0.7$ and $\alpha = 2.3$, we find $t_q^{z=1} = 30.84 > t_q^{z=2} = 25.23$ and $t_q^{sat} = 28.7$.

However, one of the above inequalities is violated for $|g| > 1$ for different anisotropy parameters. Overall, there are pairs of (g, λ) for which t_q remains almost constant with z although for some values, it fluctuates with z . On average, we find $t_q \approx [20, 30]$ in this domain of α . As expected, note that there is a critical threshold value of $\alpha \approx 5$ above which z -dependence completely vanishes.

quasi-LR regime. Again $|g| > 1$, t_q remains almost constant with z for some λ values including $\lambda = 0$. Interestingly, in this domain, one can always find a z value for which $t_q^{z=1} > t_q^{z > 1}$ (see Fig. 3(b)). On the other hand, when $|g| < 1$, and $\lambda \neq 0$, $t_q^{z > 1}$ fluctuates more and is significantly higher than $t_q^{z=1}$. One can argue that this high value of t_q is due to the entanglement-creation between any two arbitrary sites which is not the case when there is only nearest-neighbor interactions. But we will show that such a simplistic argument may not be true as low t_q can also be found in the LR domain.

$0 \leq \alpha \leq 1$ – *LR domain.* Like short- and quasi long-range models, there exists (λ, g) -pairs for which we can find some z values with $t_q^{z=1} > t_q^{z > 1}$. In these cases, the variation of t_q with z is not substantial. To capture this, we compute the average t_q over all z for a fixed α and N which we

denote as \bar{t}_q . For example, for $N = 25$, $\lambda = 0$ and $\forall g$, we find that for $\alpha = 2.5$, $\bar{t}_q = 23.82$, and for $\alpha = 1.5$, $\bar{t}_q = 87.48$ while when we use LR interacting Hamiltonian for state transfer, we obtain $\bar{t}_q = 27.89$ with $\alpha = 0.5$. At the same time, we also identify the system parameters, for which $t_q^{z=1} > t_q^{z>1} \forall z$ and the difference is substantial. For example, with $\lambda = 0.5, g = 0.2$ and $N = 25$, we notice that $t_q^{z=1} \sim \mathcal{O}(10^4)$ and $t_q^{z=24} = 42.42$. This clearly establishes the usefulness of LR interacting spin model for the state transfer scheme which naturally occurs in several physical systems. Secondly, it also illustrates that the fall-off rate and the range of interactions depend on the trade-off between entanglement-creation and -destruction required for state transmission in a complicated way.

We also observe that there exists anisotropy and magnetic field strength for which $t_q \sim \mathcal{O}(10^3)$, i.e., the minimum time required to achieve quantum advantage is almost double or triple to the one obtained for $\lambda = 0$ and other λ values with $g > 1$. Interestingly, we find some pairs of (λ, g) , i.e., tunable parameters for which t_q decreases with z , thereby exhibiting again quantum advantage of having LR interactions (see Fig. 3 (c)).

1. Better state transfer with low coordination number

From the study, it is clear that $z \leq N/2$ has a special status although they involve interactions beyond nearest neighboring sites. In this situation, t_q increases with α and saturates to a certain t_q^{sat} value irrespective of the anisotropy and magnetic field strength provided the length of the spin chain is moderate (see Fig. 4). The saturation occurs when the fall off rate, α , belongs to the short-range regimes. Precisely, the saturation of time for quantum advantage, t_q^{sat} , happens when $\alpha \gtrsim 4$ for a fixed $N \sim \mathcal{O}(50)$. This again indicates that when α is less than 4, we can surely gain by employing long-range interactions during the dynamics. When z is relatively high and close to $N/2$, some fluctuations in t_q are also observed for $\alpha \leq 2$ although $t_q^{\alpha=0} < t_q^{sat}$. This indicates that although there can be some advantages of long-range interacting systems, it becomes highly sensitive towards a successful state transfer, especially in the quasi long-range regimes as is evident from \bar{t}_q . This behavior can be explained in the following way – a successful execution of state transfer scheme depends both on the creation of entanglement between different sites including nearest-neighbor and at the same time, it is also essential to disentangle the site on which the state to be transferred. The competition between two kinds of operations, entanglement-generating and disentangling power [73], can be responsible for fluctuations in t_q when the fall-off rate is small or moderate for which the unitary operator has a high multipartite entanglement-generating capability [53, 74] compared to the system having only nearest-neighbor interactions.

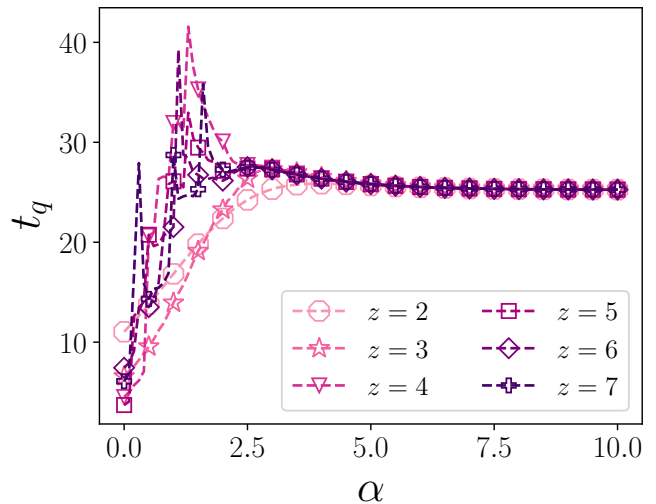


FIG. 4. The variation of time t_q (ordinate) with respect to the decay strength α (abscissa). Increasing coordination numbers z represented by a gradient from light to dark shades (with different markers), is presented, corresponding to $N = 25$, with $\lambda = 1$ and $g = 1.7$. We observe that when $z \leq N/2$, t_q required for low α is less than the one with high α although there are fluctuations in t_q with low α . t_q saturates when $\alpha \geq 4 \forall z \leq N/2$. All the axes are dimensionless.

IV. PROVIDING HIGH FIDELITY WITH VARIABLE-RANGE INTERACTING MODEL

After guaranteeing the benefit of long-range interacting Hamiltonian as evolving one with respect to minimum time to have quantum advantage, it is now natural to ask – “*can the fidelity reach a higher value for a long-range interacting model compared to short-range ones?*” In other words, is there any gain in terms of fidelity by increasing the range of interactions? We will answer this question affirmatively.

To address this question, we define a quantity, maximum fidelity which is attained for the first time beyond the classical limit and is denoted by f^* and the corresponding time is denoted by t^* . Our goal is to study how f^* depends on the variable-range interactions involved in dynamics. To examine the role of coordination number and fall-off rates, we again fix the set of parameters, λ, g and N to the values obtained after examining Fig. 2.

Dependence of coordination number. For a given N, g and λ , we first find α for which f^* does not vary with z . We observe that f^* is independent of z when $\alpha \geq 5$. This suggests that the range of interactions and fall-off rate have a significant contribution in f^* when $\alpha < 5$. We first notice that the pattern of f^* with z for different α values is quite similar to the behavior of t_q (comparing Figs. 4 and 5) – f^* first sharply increases (decreases) with z and saturates to a value, referred to as f^{*sat} . Again, $z = 2$ along with $z = 3$ turns out to be special. In particular, we find several instances when $\alpha \in [2, 4]$, where

$$f^{*z=1} < f^{*z=2}, \text{ and } f^{*z=1} < f^{*sat}. \quad (5)$$

In some cases, the increment is significant. For example, we notice that $\lambda = 1, g = 1.7, N = 25$, with $\alpha = 10$,

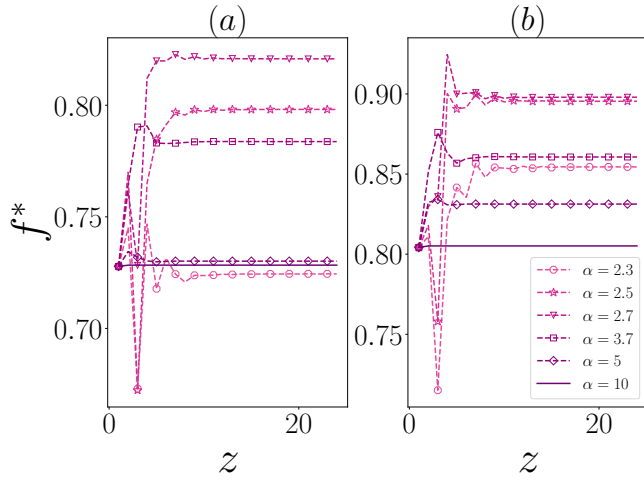


FIG. 5. The maximum fidelity f^* (vertical axis) attained for the first time beyond the classical limit as a function of the coordination number z (horizontal axis) for different fall-off rates. From the light to dark shades, α increases. Here $N = 25$. Two combinations of (λ, g) are considered – (a) $\lambda = 0.9$ and $g = 0.7$, and (b) $\lambda = 1$ and $g = 1.7$. $\alpha \geq 5$ mimics f^* with NN interacting evolving Ising Hamiltonian. Hence, low α incorporating distant range interactions can yield higher fidelity as compared to the short-range model subject to the choices of (λ, g) values. All the axes are dimensionless.

$f^{*sat} = 0.81$ while for the same set of values and for $\alpha = 2.7$, we obtain $f^{*sat} = 0.9$. Such a rise of f^* is also achieved when $\lambda \neq 0$ and $|g| < 1$, as shown in Fig. 5. As argued before, the contest between entangling and disentangling power of unitary responsible for transferring the state efficiently is lowest when $\alpha \sim 2$ which still carries the effect of range of interactions.

1. Fidelity with maximum coordination number – status of anisotropy

To scrutinize the consequence of long-range of interactions, let us consider the maximum coordination number for a fixed N , i.e., $z = N - 1$. The observations are as follows:

1. f^* is nonmonotonic with the fall off rate except for the XX model with $\lambda = 0$ (see Fig. 6) and f^* is fluctuating when $\alpha \ll 2$, irrespective of other system parameters.
2. Interestingly, f^* reaches its maximum value when $\alpha \approx 2$ and the maximum value, denoted as f^{*max} , depends on the anisotropy parameter, λ . Specifically, with $g > 1$, if one increases λ so that it is close to unity, f^* starts increasing when $\alpha \gtrsim 2$, after achieving its maximum, it decreases and finally saturates to a certain value, f^{*sat} (where f^{*sat} above is different than this f^{*sat} as it considers saturation with α while in the previous case, the saturation is observed with z), for $\alpha \gtrsim 8$.

In other words, when the evolving Hamiltonian is close to the Ising model, the nonmonotonic behavior of f^* is more

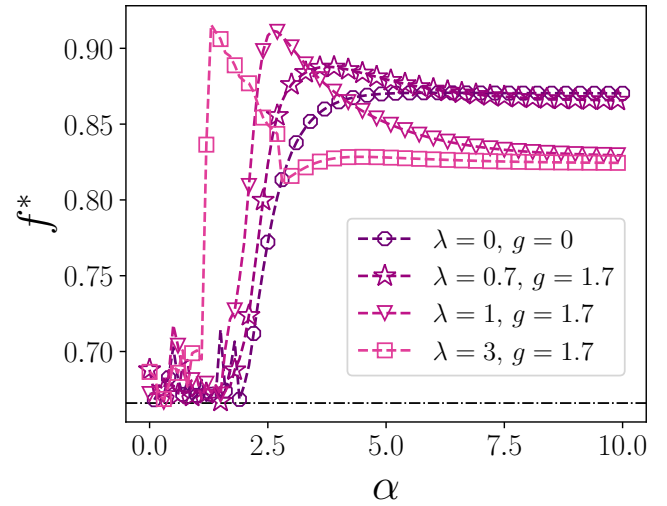


FIG. 6. Nonmonotonic behavior of f^* (ordinate) with respect to decay strength α (abscissa) of the extended transverse Ising model. Different symbols represent choices of λ and g . Here $N = 20$. It is observed that the fidelity achieves a maximum value (even beyond 0.9) for a specific value of $\alpha \sim 2$. Again for small α values, f^* fluctuates. All the axes are dimensionless.

pronounced, i.e., $\Delta_{f^*} = f^{*max} - f^{*sat}$ increases with the increase of λ . For example, for the transverse Ising model with $\lambda = 1$, $\Delta_{f^*} = 0.08$ (when $g = 1.7$ and $N = 20$) while for $\lambda = 1.3$, $\Delta_{f^*} = 0.15$. Similar nonmonotonic behavior can also be observed for other pairs of (λ, g) and $N \leq 100$. However, with the increase of N , f^* including f^{*sat} and f^{*max} decreases which will be addressed next.

A. Overcoming decline of fidelity with system-size by LR interactions

The entire investigation is performed by fixing the length of the chain and varying other system parameters. We are now interested to study how the maximum fidelity f^* decreases with the increase of N . The decaying behavior of f^* is expected as one rises the length of chain whose end points are used to place the initial and the final states.

Since our objective is to focus on the range of interactions, the maximum fidelity is examined with the length of the chain when the coordination number is maximum. Again, when we consider the XX model with nearest-neighbor interactions ($\alpha = 10$), we observe that f^* remains above the classical limit for a very high value of $N > 150$, while f^* sharply decreases with N when $\alpha \approx 2$ and it reaches the classical limit with $N \approx \mathcal{O}(100)$.

The opposite picture emerges when one rises λ , close to the Ising evolving Hamiltonian. In particular, we observe that when $\lambda = 1$, $g = 1.7$ with $\alpha = 10$, $f^* = f^{cl}$ when $N = 138$ while when one increases $\alpha \approx 2$, f^* is surely higher than the classical fidelity with the same length of the chain, i.e., $f^* > f^{cl}$ for $N > 138$.

To make the analysis more concrete, we fit the decaying curve of f^* with the function, given by $a \exp(-bN^{-\eta})$, for different α values. In order to justify the positive impact

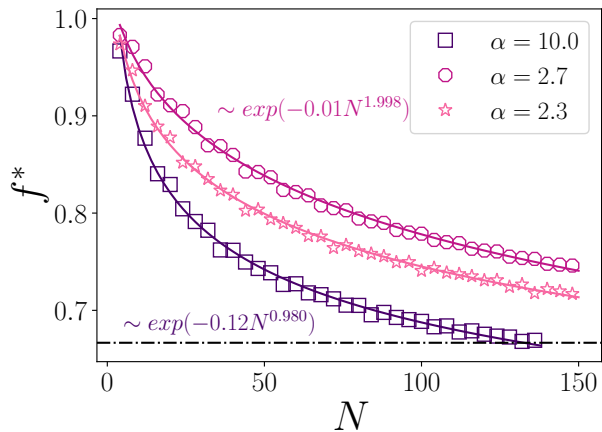


FIG. 7. The dependency of fidelity f^* (ordinate) on the system size N (abscissa) is plotted. Stars, circles, and squares represent $\alpha = 2.3, 2.7$ and 10 respectively. Here $\lambda = 1$ and $g = 1.7$. We fit the decaying curve with $a \exp(-bN^\eta)$. We find that with $a = 1$, η decreases along with the increase of b . Two observations emerge – (1) for a given N , $f^{*\alpha=10} < f^{*\alpha<10}$; (2) there exists N for which $f^{*\alpha=10}$ cannot beat the classical limit while $f^{*\alpha\sim 2}$ is much higher than the classical fidelity. All the axes are dimensionless.

of LR interactions towards combating the decline of fidelity with system-size, we find out how η and b change with the fall-off rate α for maximum coordination number. Interestingly, there are system parameters for which we notice that b increases while η decreases with the increase of α . It ensures that the rate of fall for f^* with the increase of system-size can be delayed with the introduction of LR interactions, as depicted in Fig. 7. .

V. CONCLUSION

The extended XY model with long-range interactions provides a powerful platform for investigating the feasibility of quantum state transfer (QST) protocols and exploring their potential in quantum technologies. We demonstrated that the incorporating long-range interactions in the spin chain significantly altered the dynamics of state transfer, resulting in a shorter time required to achieve quantum advantage. Specifically, it was observed that the quasi long- and long-range regimes, where the decay strength is moderately low, exhibited an optimal interplay between interaction range and efficiency, outperforming both short-range systems. Furthermore, the role of the coordination number in QST was highlighted, where intermediate coordination numbers, involving interactions beyond nearest neighbors, facilitated faster and more reliable state transfer compared to excessively high values.

The study revealed that long-range interactions had a direct impact on enhancing the maximum fidelity of state transfer, even in larger systems. While fidelity typically decreased with an increase in system size, the presence of long-range interactions reduced this decline, ensuring reliable performance in scenarios where short-range models failed to main-

tain fidelity above the classical threshold. It was also found that the interplay of anisotropy and magnetic field strength played a crucial role, with strong anisotropy enhancing fidelity at the expense of increased sensitivity to field variations, while the XX model, with a zero anisotropy limit, demonstrated robustness over a wider range of conditions.

Additionally, distinct behaviors across the long-, quasi long-, and short-range interaction regimes were uncovered. In the long-range regime, fluctuations in transfer time and fidelity were attributed to the dynamics of entanglement generating and disentangling powers of the evolving Hamiltonian, whereas the quasi long-range domain provided a stable and efficient configuration for state transfer. In contrast, the short-range interacting model closely resembled traditional nearest-neighbor ones, exhibiting diminished performance due to limited interaction range.

These findings are not only of theoretical interest but they can also be experimentally verified in state-of-the-art quantum platforms, including trapped ions, Rydberg atom arrays, and optical lattices. The parameter regimes explored in this work align well with the capabilities of these systems, where decay strength, coordination number, anisotropy, and magnetic field strength can be finely tuned. By leveraging the exotic properties of long-range interactions, this study has opened new avenues for the design of scalable and efficient quantum communication systems, either on their own or within quantum computing circuits, providing a solid foundation for future advancements in the field.

ACKNOWLEDGMENTS

We acknowledge the use of cluster computing facility at the Harish-Chandra Research Institute. This research was supported in part by the INFOSYS scholarship for senior students. LGCL received funds from project DYNAMITE QUANTERA2-00056 funded by the Ministry of University and Research through the ERANET COFUND QuantERA II – 2021 call and co-funded by the European Union (H2020, GA No 101017733). Funded by the European Union. Views and opinions expressed are however those of the author(s) only and do not necessarily reflect those of the European Union or the European Commission. Neither the European Union nor the granting authority can be held responsible for them. This work was supported by the Provincia Autonoma di Trento, and Q@TN, the joint lab between University of Trento, FBK—Fondazione Bruno Kessler, INFN—National Institute for Nuclear Physics, and CNR—National Research Council.

Appendix A: Diagonalization of XY model

Let us begin by considering a general quadratic Hamiltonian [58] in fermionic operators:

$$\hat{\mathcal{H}} = \sum_{i,j} P_{ij} \hat{f}_i^\dagger \hat{f}_j + \frac{1}{2} \sum_{i,j} (Q_{ij} \hat{f}_i^\dagger \hat{f}_j^\dagger + Q_{ij}^* \hat{f}_j \hat{f}_i) \quad (\text{A1})$$

Here, \hat{f}_i and \hat{f}_i^\dagger are fermionic annihilation and creation operators, respectively, obeying the canonical anticommutation relations, $\{\hat{f}_i, \hat{f}_j^\dagger\} = \delta_{ij}$ and $\{\hat{f}_i, \hat{f}_j\} = \{\hat{f}_i^\dagger, \hat{f}_j^\dagger\} = 0$. The matrices P and Q encode the specific properties of our system, including interaction strengths and coupling terms. To diagonalize this Hamiltonian, we introduce Bogoliubov quasiparticle operators as $\hat{\eta}_q = \sum_m (\mathcal{A}_{qm} \hat{f}_m + \mathcal{B}_{qm} \hat{f}_m^\dagger)$. The transformation matrices \mathcal{A} and \mathcal{B} are chosen such that the Hamiltonian becomes diagonal in the new basis $\hat{\mathcal{H}} = \sum_q \epsilon_q \hat{\eta}_q^\dagger \hat{\eta}_q$, where ϵ_q represents the quasiparticle energies. This diagonalization is crucial for understanding the system's excitation spectrum and its response to perturbations.

Now, let us connect this general form to our specific spin system. We can map our spin-1/2 operators to fermionic operators using the Jordan-Wigner transformation. This well-known transformation can be expressed as $\hat{S}_j^+ = \hat{f}_j^\dagger \prod_{i<j} (1 - 2\hat{f}_i^\dagger \hat{f}_i)$, $\hat{S}_j^- = \hat{f}_j \prod_{i<j} (1 - 2\hat{f}_i^\dagger \hat{f}_i)$, $\hat{S}_j^z = \hat{f}_j^\dagger \hat{f}_j - \frac{1}{2}$, where $\hat{S}_j^\pm = \hat{S}_j^x \pm i\hat{S}_j^y$ are the spin raising and lowering operators. The string operator $\prod_{i<j} (1 - 2\hat{f}_i^\dagger \hat{f}_i)$ ensures the correct anticommutation relations between operators at different sites, maintaining the non-local nature of the spin algebra in the fermionic representation. Applying this transformation to our spin Hamiltonian yields Eq. (3) [58–60].

To study the dynamics, we work in the Heisenberg picture. The time evolution of the fermionic operators for a given site m is given by

$$\hat{f}_m(t) = e^{i\hat{\mathcal{H}}t} \hat{f}_m e^{-i\hat{\mathcal{H}}t} = \sum_{k=0}^N [\Phi_{mk}(t) \hat{f}_k + \Psi_{mk}(t) \hat{f}_k^\dagger], \quad (\text{A2})$$

Here the time-dependent coefficients $\Phi(t)$ and $\Psi(t)$ are determined by the Bogoliubov transformation, $\Phi(t) = \mathcal{A}^T e^{-i\epsilon t} \mathcal{A} + \mathcal{B}^T e^{i\epsilon t} \mathcal{B}$ and $\Psi(t) = \mathcal{A}^T e^{-i\epsilon t} \mathcal{B} + \mathcal{B}^T e^{i\epsilon t} \mathcal{A}$. These equations provide a complete description of the system's time evolution, allowing us to calculate various observables and study both equilibrium and non-equilibrium properties of the system.

Appendix B: Computation of fidelity

This appendix outlines the derivation of fidelity f for quantum information transfer in systems with long-range interactions, building upon the framework presented in Ref. [71]. Let Λ be a quantum channel that describes the evolution of the density matrix from the qubit at $t = 0$ to the resulting qubit at time t as $\sigma(t) = \Lambda[\sigma(0)]$. The fidelity f which characterizes the channel's efficiency is defined as [75] $\Omega(t) = \max_{V \in U(2)} \int d\phi_i \langle \phi_i | V^\dagger \Lambda[|\phi_i\rangle \langle \phi_i|] V | \phi_i \rangle$, where V is the local unitary operation. For systems governed by anisotropic exchange interactions, assuming conservation of excitation number and focusing on the Bloch sphere mapping from the initial to the resulting qubit such that the corresponding fidelity can be expressed as $f = \frac{1}{2} + \frac{1}{6} |p(t)^2 - q(t)^2| + \frac{1}{3} \max\{p(t), q(t)\}$, where $p(t) = |\Phi_{N0}(t)|$ and $q(t) = |\Psi_{N0}(t)|$ are time-dependent coefficients related to the transfer process. The coefficients $p(t)$ and $q(t)$ are determined by the system's Hamiltonian parameters and incorporate the effects of long-range interactions.

-
- [1] C. H. Bennett, G. Brassard, C. Crépeau, R. Jozsa, A. Peres, and W. K. Wootters, *Phys. Rev. Lett.* **70**, 1895 (1993).
 - [2] J.-W. Pan, D. Bouwmeester, M. Daniell, H. Weinfurter, and A. Zeilinger, *Nature* **403**, 515 (2000).
 - [3] N. Kumar, I. Kerenidis, and E. Diamanti, *Nat. Commun.* **10**, 1 (2019).
 - [4] M. Hillery, V. Bužek, and A. Berthiaume, *Phys. Rev. A* **59**, 1829 (1999).
 - [5] N. Gisin, G. Ribordy, W. Tittel, and H. Zbinden, *Rev. Mod. Phys.* **74**, 145 (2002).
 - [6] R. Alicki and M. Fannes, *Phys. Rev. E* **87**, 042123 (2013).
 - [7] F. Campaioli, S. Gherardini, J. Q. Quach, M. Polini, and G. M. Andolina, *Rev. Mod. Phys.* **96**, 031001 (2024).
 - [8] C. L. Degen, F. Reinhard, and P. Cappellaro, *Rev. Mod. Phys.* **89**, 035002 (2017).
 - [9] L. Pezzè, A. Smerzi, M. K. Oberthaler, R. Schmied, and P. Treutlein, *Rev. Mod. Phys.* **90**, 035005 (2018).
 - [10] S. Bose, *Phys. Rev. Lett.* **91**, 207901 (2003).
 - [11] V. Subrahmanyam, *Phys. Rev. A* **69**, 034304 (2004).
 - [12] G. M. A. Almeida, *Phys. Rev. A* **98**, 012334 (2018).
 - [13] Y. Li, T. Shi, B. Chen, Z. Song, and C.-P. Sun, *Phys. Rev. A* **71**, 022301 (2005).
 - [14] V. Giovannetti and D. Burgarth, *Phys. Rev. Lett.* **96**, 030501 (2006).
 - [15] Z. Jiang, Q. Chen, and S. Wan, *Phys. Rev. A* **76**, 034302 (2007).
 - [16] B. Chen, Z. Song, and C. P. Sun, *Phys. Rev. A* **75**, 012113 (2007).
 - [17] O. Romero-Isart, K. Eckert, and A. Sanpera, *Phys. Rev. A* **75**, 050303 (2007).
 - [18] D. Burgarth, V. Giovannetti, and S. Bose, *Phys. Rev. A* **75**, 062327 (2007).
 - [19] A. Kay, *Int. J. Quantum Inform.* **08**, 641 (2010).
 - [20] N. Y. Yao, L. Jiang, A. V. Gorshkov, Z.-X. Gong, A. Zhai, L.-M. Duan, and M. D. Lukin, *Phys. Rev. Lett.* **106**, 040505 (2011).
 - [21] R. Yousefjani and A. Bayat, *Phys. Rev. A* **102**, 012418 (2020).
 - [22] T. J. G. Apollaro, S. Lorenzo, F. Plastina, M. Consiglio, and K. Życzkowski, *Entropy* **25**, 46 (2022).
 - [23] C. Jameson, B. Basyildiz, D. Moore, K. Clark, and Z. Gong, *Quantum Sci. Technol.* **9**, 015014 (2023).
 - [24] Y. Xu, D. Zhu, F.-X. Sun, Q. He, and W. Zhang, *New J. Phys.* **25**, 113015 (2023).
 - [25] N. E. Palaiodimopoulos, M. Kiefer-Emmanouilidis, G. Kurizki, and D. Petrosyan, *SciPost Phys. Core* **6**, 017 (2023).
 - [26] L. Huang, M. Deng, C. Sun, and F. Li, *Phys. Rev. B* **110**, 014303 (2024).
 - [27] C. Albanese, M. Christandl, N. Datta, and A. Ekert, *Phys. Rev. Lett.* **93**, 230502 (2004).
 - [28] M. Christandl, N. Datta, T. C. Dorlas, A. Ekert, A. Kay, and A. J. Landahl, *Phys. Rev. A* **71**, 032312 (2005).

- [29] D. Burgarth, V. Giovannetti, and S. Bose, *J. Phys. A: Math. Gen.* **38**, 6793 (2005).
- [30] A. Kay, *Phys. Rev. A* **73**, 032306 (2006).
- [31] C. Di Franco, M. Paternostro, and M. S. Kim, *Phys. Rev. Lett.* **101**, 230502 (2008).
- [32] P. Karbach and J. Stolze, *Phys. Rev. A* **72**, 030301 (2005).
- [33] G. Gualdi, V. Kostak, I. Marzoli, and P. Tombesi, *Phys. Rev. A* **78**, 022325 (2008).
- [34] G. Gualdi, I. Marzoli, and P. Tombesi, *New J. Phys.* **11**, 063038 (2009).
- [35] Z. C. Shi, X. L. Zhao, and X. X. Yi, *Phys. Rev. A* **91**, 032301 (2015).
- [36] C. B. Pushpan, H. K. J., and A. K. Pal, *Phys. Lett. A* **511**, 129543 (2024).
- [37] T. Anuradha, A. Patra, R. Gupta, and A. S. De, “Perfect transfer of arbitrary continuous variable states across optical waveguide lattices,” (2023), arXiv:2306.13068 [quant-ph].
- [38] Y.-Q. Wang, M.-S. Wei, M.-J. Liao, Z.-J. Lin, S.-L. Wang, J. Xu, and Y. Yang, *Phys. Rev. A* **110**, 063525 (2024).
- [39] X.-Q. Liu, J. Liu, and Z.-Y. Xue, *JETP Lett.* **117**, 859 (2023).
- [40] R. M. Nandkishore and S. L. Sondhi, *Phys. Rev. X* **7**, 041021 (2017).
- [41] D. V. Else, F. Machado, C. Nayak, and N. Y. Yao, *Phys. Rev. A* **101**, 022333 (2020).
- [42] N. Defenu, T. Donner, T. Macrì, G. Pagano, S. Ruffo, and A. Trombettoni, *Rev. Mod. Phys.* **95**, 035002 (2023).
- [43] A. Solfanelli, G. Giachetti, M. Campisi, S. Ruffo, and N. Defenu, *New J. Phys.* **25**, 033030 (2023).
- [44] S. Puri, T. K. Konar, L. G. C. Lakkaraju, and A. S. De, “Floquet driven long-range interactions induce super-extensive scaling in quantum battery,” (2024), arXiv:2412.00921 [quant-ph].
- [45] R. Yousefjani, X. He, and A. Bayat, *Chin. Phys. B* **32**, 100313 (2023).
- [46] Monika, L. G. C. Lakkaraju, S. Ghosh, and A. S. De, “Better sensing with variable-range interactions,” (2023), arXiv:2307.06901 [quant-ph].
- [47] I. Bloch, *J. Phys. B: At. Mol. Opt. Phys.* **38**, S629 (2005).
- [48] D. A. Abanin, E. Altman, I. Bloch, and M. Serbyn, *Rev. Mod. Phys.* **91**, 021001 (2019).
- [49] J. Gliozzi, J. May-Mann, T. L. Hughes, and G. De Tomasi, *Phys. Rev. B* **108**, 195106 (2023).
- [50] Z. Eldredge, Z.-X. Gong, J. T. Young, A. H. Moosavian, M. Foss-Feig, and A. V. Gorshkov, *Phys. Rev. Lett.* **119**, 170503 (2017).
- [51] M. C. Tran, C.-F. Chen, A. Ehrenberg, A. Y. Guo, A. Deshpande, Y. Hong, Z.-X. Gong, A. V. Gorshkov, and A. Lucas, *Phys. Rev. X* **10**, 031009 (2020).
- [52] S. Hermes, T. J. G. Apollaro, S. Paganelli, and T. Macrì, *Phys. Rev. A* **101**, 053607 (2020).
- [53] M. C. Tran, A. Y. Guo, A. Deshpande, A. Lucas, and A. V. Gorshkov, *Phys. Rev. X* **11**, 031016 (2021).
- [54] Y. Hong and A. Lucas, *Phys. Rev. A* **103**, 042425 (2021).
- [55] X. Wang, J.-Q. Li, T. Liu, A. Miranowicz, and F. Nori, *Phys. Rev. Res.* **6**, 043226 (2024).
- [56] D. Vodola, L. Lepori, E. Ercolessi, and G. Pupillo, *New Journal of Physics* **18**, 015001 (2015).
- [57] D. Vodola, L. Lepori, E. Ercolessi, A. V. Gorshkov, and G. Pupillo, *Phys. Rev. Lett.* **113**, 156402 (2014).
- [58] E. Lieb, T. Schultz, and D. Mattis, *Annals of Physics* **16**, 407 (1961).
- [59] E. Barouch, B. M. McCoy, and M. Dresden, *Phys. Rev. A* **2**, 1075 (1970).
- [60] E. Barouch and B. M. McCoy, *Phys. Rev. A* **3**, 786 (1971).
- [61] S. Sachdev, *Quantum Phase Transitions* (Cambridge University Press, 2009).
- [62] K. Blekos, D. Brand, A. Ceschini, C.-H. Chou, R.-H. Li, K. Pandya, and A. Summer, *Physics Reports* **1068**, 1 (2024), a review on Quantum Approximate Optimization Algorithm and its variants.
- [63] X. Xu, Manabputra, C. Vignes, M. H. Ansari, and J. M. Martinis, *Phys. Rev. Appl.* **22**, 064030 (2024).
- [64] E. Pelofske, A. Bäertschi, and S. Eidenbenz, in *High Performance Computing*, edited by A. Bhatlele, J. Hammond, M. Baboulin, and C. Kruse (Springer Nature Switzerland, Cham, 2023) pp. 240–258.
- [65] E. Pelofske, A. Bäertschi, and S. Eidenbenz, *npj Quantum Inf.* **10**, 1 (2024).
- [66] N. Linden, S. Popescu, and P. Skrzypczyk, *Phys. Rev. Lett.* **105**, 130401 (2010).
- [67] S. Massar and S. Popescu, *Phys. Rev. Lett.* **74**, 1259 (1995).
- [68] D. Burgarth, *Eur. Phys. J. Spec. Top.* **151**, 147 (2007).
- [69] T. Koffel, M. Lewenstein, and L. Tagliacozzo, *Phys. Rev. Lett.* **109**, 267203 (2012).
- [70] P. Hauke and L. Tagliacozzo, *Phys. Rev. Lett.* **111**, 207202 (2013).
- [71] A. Bayat, L. Banchi, S. Bose, and P. Verrucchi, *Phys. Rev. A* **83**, 062328 (2011).
- [72] L. G. C. Lakkaraju, S. Ghosh, D. Sadhukhan, and A. Sen(De), *Phys. Rev. A* **106**, 052425 (2022).
- [73] L. Clarisse, S. Ghosh, S. Severini, and A. Sudbery, *Physics Letters A* **365**, 400 (2007).
- [74] P. Zanardi, *Phys. Rev. A* **63**, 040304 (2001).
- [75] M. Horodecki, P. Horodecki, and R. Horodecki, *Phys. Rev. A* **60**, 1888 (1999).